IEEE Access
Multidisciplinary | Rapid Review | Open Access Journal

Received 29 September 2023, accepted 15 October 2023, date of publication 19 October 2023, date of current version 25 October 2023.

*Digital Object Identifier 10.1109/ACCESS.2023.3325840*

RESEARCH ARTICLE

# Adaptive Active Generator Torque Controller Design Using Multi-Objective Optimization for Tower Lateral Load Reduction in Monopile Offshore Wind Turbines

**MANUEL LARA[1], FRANCISCO VÁZQUEZ[1], IÑAKI SANDUA-FERNÁNDEZ[2], AND JUAN GARRIDO[1]**

[1]Department of Electrical Engineering and Automation, University of Cordoba, Campus of Rabanales, 14071 Cordoba, Spain
[2]Wind Energy Department, National Renewable Energy Centre (CENER), Sarriguren, 31621 Navarra, Spain

Corresponding author: Juan Garrido (juan.garrido@uco.es)

This work was supported in part by the Spanish Ministry of Science and Innovation under Grant PID2020-117063RB-I00/AEI/10.13039/501100011033; and in part by the Regional Government of Andalusia, Spain, under Grant 1380282-R. The work of Manuel Lara was supported by the FPU Fellowship from the Spanish Ministry of Education, Culture, and Sports under Grant FPU17/02747.

**ABSTRACT** The study of fatigue load reduction in wind turbines has gained significant interest in recent years. In monopile offshore wind turbines, vibrations induced by misalignment between waves and wind directions can considerably shorten the tower's lifespan due to lateral loads. To cope with this issue, this work focuses on the design and evaluation of control strategies to mitigate these loads. An adaptive active generator torque control (AGTC) scheme is proposed to mitigate lateral tower fatigue within the nominal region. Two variants of AGTC are suggested: with or without using a bandpass filter. A multi-objective optimization using genetic algorithms is employed to determine the optimal AGTC parameters based on wind speed and wave height. Objective functions related to tower and low-speed shaft fatigue load reduction, as well as power fluctuation minimization, are employed. The performance of the proposed AGTC controllers is assessed in comparison to a baseline controller. The results highlight that the AGTC strategy without a filter effectively reduces lateral tower fatigue load at the expense of higher power signal oscillations and increased fatigue in the low-speed shaft. Using a filter in the AGTC mitigates these adverse effects, smoothing power oscillations to achieve similar values as the baseline control, and significantly reducing the load experienced in the low-speed shaft. The proposed methodology is robust and adaptable to various wind and wave conditions, demonstrating its ability to enhance the structural integrity of wind turbines without compromising power generation efficiency.

**INDEX TERMS** Wind turbines, active generator torque control, lateral tower vibration reduction, multi-objective optimization, genetic algorithms, active tower damping control.

## I. INTRODUCTION

Wind energy has experienced tremendous growth over the past decade, which has helped push renewables into direct competition with traditional fuel-based energy. In 2021 the European Union presented a new climate action plan to reduce greenhouse gas emissions by at least 55% by 2030. This plan includes increased investment in wind and solar energy, with onshore and offshore wind energy expected to account for a quarter of the EU's renewable energy generation capacity by 2030 [1]. The increase in clean energy production is expected to continue to rise over the next few years to reach almost 50% of the electricity demanded by 2050 [2]. The main development of wind energy technology

The associate editor coordinating the review of this manuscript and approving it for publication was Ahmed F. Zobaa.

in recent decades has been related to the growth of wind turbine size, helping to increase power output and energy efficiency, but creating challenges in wind turbine operation and maintenance. In recent years, advanced control approaches have been developed that focus on maximizing power output, mitigating structural loads, and extending wind turbine life [3]. These objectives often conflict when designing a wind turbine control system, and the trade-off between them varies and depends on actual operating situations, such as wind characteristics, system aging, and grid requirements.

Currently, three-bladed horizontal axis wind turbines with variable speed and variable blade pitch (VS-VP) are the most common because they can optimize power generation at various wind speeds [4]. These wind turbines operate in different regions depending on the wind speed: connection (I), partial load (II), transition (III), full load (IV) and disconnection (V), as shown in Fig. 1, which shows the ideal power curve of a wind turbine.

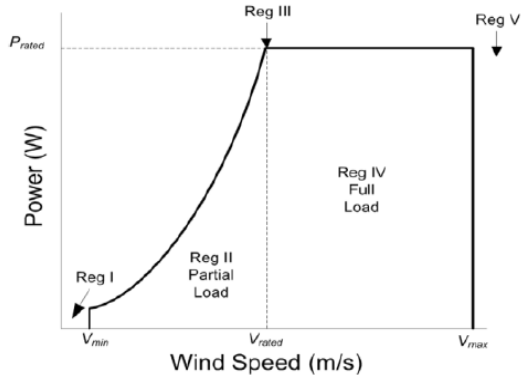


**FIGURE 1.** Operation regions of a wind turbine.

This work focuses on the full load region (Reg. IV), where the impact of high wind speed must be minimized to avoid damage to the system. Here it is necessary to keep the generator power and, consequently, the generator speed at their rated values, which is achieved by using controllers that modify the pitch angle of the blades to adjust the aerodynamics of the wind turbine and limit the amount of energy removed from the wind [5]. Normally, these controllers send the same pitch value to all three blades, which is called collective pitch control (CPC). In this region, the generated power ($P_g$) usually depends only on the generator speed, $\omega_g$, according to (1) since the generator torque remains constant at its rated value $T_{g,rated}$.

$$P_{g,rated} = T_{g,rated} \cdot \omega_{g,rated} \tag{1}$$

Although PID controllers are traditionally used to regulate the pitch angle, computational intelligence methods are a growing alternative for solving wind turbine control problems. In [6], the authors propose a hybrid control scheme that combines a PID controller with a reinforcement learning-based regulator for CPC, and they achieve reducing the error of the power output compared with a PID controller. In [7], a hybrid pitch control was developed that combines a fuzzy logic controller and a deep learning module, which is in charge of estimating the effective wind. In [8], a reinforcement learning-based fuzzy adaptive optimal controller is designed for maximum power point tracking within a variable-speed wind energy generation system, enhancing robustness against uncertainties and disturbances. Methods such as artificial neural networks (ANNs) and Genetic Algorithms (GAs) are well known computational tools to improve the performance of control techniques [9]. In [10], an ANN is implemented as a pitch controller to regulate the output power at the nominal value. In [11], an innovative pitch neuro-control system is presented, employing neural networks that dynamically adapt to environmental fluctuations, thereby enhancing control performance in contrast to conventional PID controllers.

Wind turbines are vulnerable to external vibrations, such as wind, wave, and seismic loads, which can affect wind energy conversion and decrease the lifetime of their structural components. Even in extreme situations, excessive vibrations can lead to catastrophic collapse of the wind turbine [3]. The complexity of dynamic behaviours, such as aerodynamics, blade rotation, and ground-structure interaction, makes it difficult to mitigate adverse vibrations. To maintain the structural safety and serviceability of wind turbines, it is necessary to mitigate these adverse vibrations and reduce structural loads to avoid premature system failure. Deflections in the tower and rotor blades, as well as vibrations in the turbine drivetrain, are the most common loads that can cause structural stresses [4].

Deflections in a wind turbine tower are usually divided in two main directions: fore-aft (in wind direction) and side-side (perpendicular to wind direction). Most of the research published to date focuses on mitigating tower fore-aft vibrations, as they are usually the most important. The different vibration control methods to reduce tower oscillations can be classified as passive, semi-active, or active [12]. In [13], passive vibration control of a spar-type floating offshore wind turbine tower using passive tuned mass-damper-inerter was investigated in detail. In [14] finite element structural analysis was combined with a semi-active tuned mass damper (TMD) to reduce the longitudinal vibration of an offshore wind turbine supported by a monopile tower. In [15], a control scheme was proposed to reduce wave-induced fatigue loads on offshore wind turbine support structures by increasing both damping and stiffness of fore-aft vibration modes. In [16], a design method is proposed for a pitch controller with active tower fore-aft damping, which improves system performance by reducing both tower fore-aft load and vibration. In [17], an intelligent control system based on fuzzy logic is tuned by GAs for an offshore wind turbine, maintaining rated power and reducing frontal vibrations. In [18], CPC is combined with an active tower damping control (ATDC) that uses feedback to inject damping into the system by means of an extra pitch controller.

For onshore turbines, the side-side fatigue loads of the tower are usually less significant compared to those in the fore-aft direction. The fore-aft component is higher since it is mainly affected by the wind, whereas the side-side component is almost unaffected by disturbances. In contrast, the support structure of offshore wind turbines can experience significant fatigue loads in the side-side direction [19]. The loads on an offshore wind turbine are introduced from stochastic processes, such as wind and waves, whose characteristics and, especially, their directions change rapidly. In general, waves are inert to rapid changes, whereas the turbulent wind can change its profile on very short time scales. Therefore, wind and wave loads often act from different directions. In particular, misalignment between waves and wind induces side-side motion due to low aerodynamic damping. Cases of pronounced misalignment between waves and wind can introduce a significant amount of fatigue damage in the side-side direction [20]. This effect can be observed in offshore wind farms in operation, such as in [21], where recorded wind and wave data from two marine sites are shown.

To reduce fatigue loads in the lateral direction it is necessary to introduce additional damping in this direction. Some investigations using passive control methods have been carried out to reduce lateral tower vibrations. In [22], a spring pendulum pounding tuned mass damper was developed to mitigate the lateral response of monopile offshore wind turbines. In [23], the performance of full-scale tuned liquid dampers to mitigate lateral tower vibrations of multimegawatt wind turbines was evaluated using real-time hybrid testing. These types of devices can be fully passively or semi-actively controlled [24].

One of the predominant control strategies for reducing lateral tower vibrations for a wind turbine is active generator torque control (AGTC) [25]. The generator torque affects the lateral motion of the structure through the reaction in the generator stator, which is attached to the main frame at the top of the tower. Therefore, it is possible to increase the damping of the side-to-side vibration modes of the structure by controlling the generator torque in the opposite phase with the side-to-side velocity. The damping is increased by a generator roll moment that counteracts the side-to-side vibrations. As examples of AGTC, in [26] AGTC was proposed to reduce lateral tower vibrations. In [27], a fuzzy torque control and a pitch sliding mode controller were developed to simultaneously mitigate output power fluctuations and lateral tower oscillations.

In [26] and [27], active vibration control using generator torque is studied, making it clear that there is a trade-off between reduction of tower lateral oscillations and output power fluctuations, since any fluctuation in generator torque, in turn, causes fluctuations in output power. However, these papers either directly ignore or very tersely study other side effects of the use of AGTC, such as increased fatigue loads on drivetrain components such as the main shaft and gearbox [20].

To our knowledge, there is no research work that simultaneously addresses the minimization of the fluctuations of the generated power, the mitigation of the lateral fatigue loads suffered in the tower and in the main shaft of the wind turbines. Reaching a compromise between these three objectives is necessary, and this is the focus of this work, which proposes the design of an adaptive controller that mitigates the lateral fatigue loads of the tower in the nominal region taking into account the other objectives mentioned above. To address this existing gap in this field of research, a CPC is combined with an AGTC in a two-loop control scheme, and the parameters of the AGTC controller are tuned with a multi-objective optimization with genetic algorithms. The proposed optimization considers an objective function of the generated power fluctuations and two objective indices associated with the tower lateral fatigue load and the low-speed shaft load (LSS). The proposed methodology is applied to a 15 MW wind turbine, which is simulated using OpenFAST and MATLAB/Simulink software. Because of the nonlinearity of the system, the AGTC control is designed adaptively with scheduled gain as a function of wind speed and recorded lateral wave height. Different AGTC schemes are compared according to whether or not they include the addition of a second-order bandpass filter.

The main novelties of this work with respect to the existing literature are:

- In previous research work directly related to [26] and [27], the AGTC strategy applied on the 5 MW NREL offshore and onshore turbine is studied, analysing the lateral displacements of the tower, generated power and torque without analysing the fatigue load on other main elements such as the drive shaft or the blades. In this work, the advantages and disadvantages of AGTC control are shown in more detail. Specifically, the influence of AGTC on the drive shaft is further studied from the viewpoint of the fatigue load experienced on the low-speed shaft.
- It is shown that the use of a well-tuned bandpass filter in AGTC brings significant improvements in the control targets set versus AGTC without a filter.
- Most of the papers published to date on OpenFAST focus on the 5 MW NREL turbine. This work is developed on a 15 MW monopile offshore turbine, a turbine on which few studies have been conducted to date.
- A multi-objective control methodology is proposed in which, through Pareto fronts, optimal solutions are shown according to the established objectives. This methodology allows the plant control operator to decide, after studying the turbine used and environmental conditions, the tuning of the parameters of the established control loops. It looks for a compromise between objectives or gives more or less priority to certain objectives, depending on technical-economic specifications that may exist.

The article has the following structure: Section II introduces some background on multi-objective optimization

and its use in wind turbines. Section III explains the proposed methodology detailing the turbine model used, the proposed adaptive AGTC scheme, the formulation of the multi-objective optimization problem, and the Pareto fronts obtained. The simulation results of the proposed controllers are evaluated in Section IV. Finally, conclusions are summarized in Section V.

## II. BACKGROUND IN MULTI-OBJECTIVE OPTIMIZATION IN WIND TURBINES

In multi-objective optimization (MOO) problems, several optimal solutions can be found within a set of conflicting objectives. Pareto fronts are a mathematical tool to visualize and analyse the optimal solutions of this type of problem as they are a graphical representation of the solutions that satisfy all the constraints of the problem and that are optimal in terms of multiple competing objectives [28], [29]. The Pareto front shows solutions that cannot be improved in one of the objectives without worsening at least one of the others.

Figure 2 shows a representative example of a Pareto front. The framed points represent feasible solutions to an optimization problem with two objectives. Smaller values are preferred over larger values; in other words, the smaller the objective functions $F_1$ and $F_2$ for each alternative, the better the option. Point C is dominated by both point A and point B for both criteria ($F_1(A) < F_1(C)$, $F_1(B) < F_1(C)$, $F_2(A) < F_2(C)$ and $F_2(B) < F_2(C)$); therefore, point C cannot be part of the Pareto front. Points A and B are on the Pareto front because they are not exclusively dominated by any other.

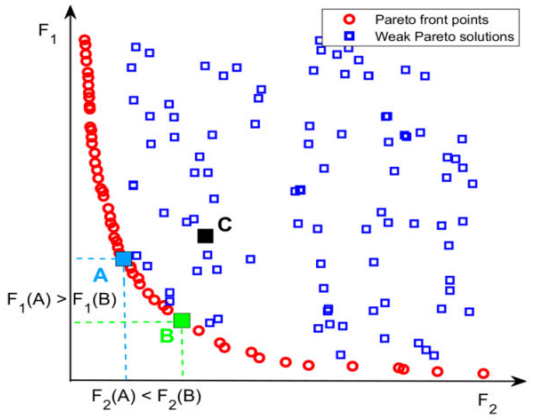


**FIGURE 2.** Example of Pareto front.

MOO problems are frequently solved using evolutionary algorithms, such as genetic algorithms, because they provide practical advantages over classical optimization techniques [30]. At the expense of numerous iterations and computing efforts, GA-based approaches can be used to identify proper and accurate Pareto fronts independently of objectives and constraint functions [31]. To achieve better computational efficiency, a fast elitist nondominated sorting genetic algorithm (NSGA-II) was designed in 2002 [32], especially for MOO.

Recent research employs MOO approaches to improve wind turbine control in simulated models. A multi-objective optimization was developed in [33] to design the control on the 5 MW NREL onshore wind turbine based on several objectives. In [34], an advanced reinforcement learning-based yaw control approach was developed combining particle swarm optimization with Pareto-based algorithms to find the optimal actions to meet the trade-off between power gain and mechanical loads resulting from yaw rotation. In [35], drive chain active damping control is designed using an optimization method and Pareto-based techniques. In other cases, coordinated control methodologies based on model predictive control together with Pareto optimization have been proposed to reduce mechanical loads and improve power output [36], [37], [38].

Other works use MOO applied in more classical control methodologies such as PID controllers. For example, in [39], MOO is used to design CPC for power performance, ATDC for tower oscillations, and individual pitch control for blade loads; the work by [40] proposes a gain scheduling PI controller for CPC, an adaptive gain for ATDC, and an adaptive feedforward compensation for the wind speed.

In situations where different goals are interrelated and cannot be achieved at the same time, an optimal solution may differ from a satisfactory solution. Generally, some objectives fall within the Pareto frontier and all the solutions on this frontier are optimal. However, a high-level optimization objective is required to analyse the optimal solutions and select the satisfactory one. Pareto frontier solutions can be evaluated and ranked using multi-criteria decision making (MCDM) methods to choose one of them based on preferences.

MCDM techniques help to compare different options based on different criteria to find the best solutions. Each method has its pros and cons; however, the choice of an approach depends on the criteria chosen. As a result, decision-makers are not bound by a single method and can use different methods to achieve non-identical results. In such cases, integrated methods are required for the final decision. MCDM methods are becoming increasingly popular for solving renewable energy problems because they involve multiple and frequently conflicting criteria. In [41], the decision-making process in multi-objective wind turbine problems is examined. The Technique for Order of Preference by Similarity to Ideal Solution (TOPSIS) is a common MCDM method used in the energy field in several studies [42], [43], [44], [45]. The TOPSIS method defines two points: the positive ideal solution, which minimizes the cost criterion, and the negative ideal solution, which maximizes the cost criterion. TOPSIS then selects as the best compromise solution the one with the shortest Euclidean distance from the positive ideal solution and the farthest Euclidean distance from the negative ideal solution [46].

## III. PROPOSED METHODOLOGY

### A. WIND TURBINE MODEL AND ENVIRONMENTAL SCENARIOS FOR OPTIMIZATION

The AGTC design methodology proposed in this paper has been applied to the International Energy Agency (IEA) Wind 15-Megawatt Reference Wind Turbine [47], which is co-simulated using MATLAB/Simulink software in conjunction with OpenFAST software [48], an open source aero-servo-hydro-elastic simulation tool developed by the National Renewable Energy Laboratory (NREL). Specifically, the proposed control system is modelled with Simulink whereas the wind turbine (tower, blades, rotor and so on) and the wind and wave profiles are modelled using OpenFAST. Both applications share the necessary data during simulation through a dynamic-link library. Although this turbine has recently been receiving more attention in the literature [49], [50], the number of research studies on this 15 MW turbine model is still scarce compared to the NREL 5 MW wind turbine [51]. In [52] a control strategy based on the combined action of a resonant controller and an individual pitch control was validated in a 15 MW IEA wind turbine supported by a semi-submersible platform. In [53], a power control strategy combining fuzzy sliding mode control with additional pitching-rate feedback was proposed for the IEA 15 MW offshore floating semi-submersible Wind Turbine. In this work, the IEA 15 MW turbine is configured in its monopile offshore mode as shown in Fig. 3. The main specifications of the turbine are shown in Table 1.

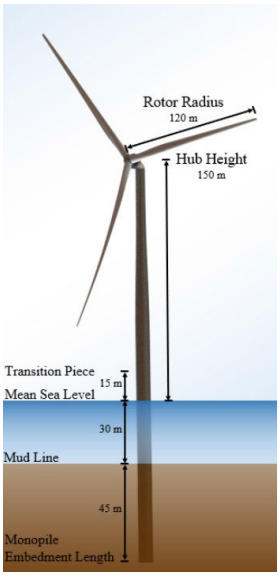


**FIGURE 3.** The IEA Wind 15-MW reference wind turbine in monopile offshore mode [47].

Considering the modularization framework of OpenFAST, the wind turbine can be modelled by the generalized nonlinear time-domain model given in (2), which represents a set of semi explicit differential algebraic equation of index 1 [54]. X() represents the continuous-state functions

**TABLE 1.** Properties of the IEA 15 MW wind turbine.

| Property | Value |
|---|---|
| Rated Power | 15 MW |
| Rotor orientation, configuration | Upwind, 3 blades |
| Cut-In, Rated Rotor Speed | 5 rpm, 7.56 rpm |
| Cut-In, Rated, Cut-Out Wind Speed | 3 m/s, 10.59 m/s, 25 m/s |
| Drivetrain | Low speed. Direct drive |
| Rated Generator Torque | 19786767.5 Nm |
| Electrical Generator Efficiency | 95.756% |
| Rotor, Hub Diameter | 240 m, 7.94 m, 150 m |
| Rotor Nacelle Assembly Mass | 1070000 kg |
| Tower Mass | 860000 kg |
| Limits on the blade pitch angle | $0 - \pi/2$ rad |
| Slew-rate limits on the pitch actuator | 0.0349 rad/s |
| Slew-rate limits on the generator torque | 4500000 Nm/s |

that determine the first-time derivatives of the continuous states **x**, which may include displacements and velocities of different structural elements. Z() are the constraint-state functions that determine the constraint (algebraic) states **z**, such as quasi-steady induction in blade element momentum theory. Y() are the output functions that determine explicitly the module-level outputs **y**, and **u** are the module-level inputs (derived from module-level outputs). Outputs and inputs may include controller commands, motions, and loads. The parameters that characterize the functions, such as geometry, mass, stiffness, aerodynamic and hydrodynamic coefficients, are represented by **p**.

$$\begin{cases} \dot{\boldsymbol{x}} = \mathrm{X}\left(\boldsymbol{x}, z, \boldsymbol{u}, t, \boldsymbol{p}\right) \\ 0 = \mathrm{Z}\left(\boldsymbol{x}, z, \boldsymbol{u}, t, \boldsymbol{p}\right) \\ \boldsymbol{y} = \mathrm{Y}\left(\boldsymbol{x}, z, \boldsymbol{u}, t, \boldsymbol{p}\right) \end{cases} \tag{2}$$

When working with offshore structures, it is crucial to consider not only the effect of wind but also the effect of waves and their contribution to fatigue damage. In addition, it is important to include wind/wave misalignment to obtain reliable estimates of cumulative fatigue damage resulting from side-side vibrations. This study focuses on the side-side vibration damping of an offshore turbine tower considering two scenarios according to the waves. The most favourable case occurs when there are no wave loads acting on the tower in the lateral direction. The most unfavourable scenario for the study occurs when wave loads act on the tower in the lateral direction perpendicular to the mean wind speed to fully excite the lateral vibration of the tower. Because of the relatively shallow water, waves occasionally refract and tend to propagate orthogonal to the sea floor contours, which means that sometimes the direction of wave propagation can be orthogonal to the mean wind speed. This loading scenario is not expected to occur as frequently as in the unidirectional case. However, if an offshore wind farm with numerous wind turbines is considered, there is a strong likelihood that there will always be a specific number of wind turbines in such a situation [21], [26].

The OpenFAST software is used to generate irregular waves according to the following JONSWAP/Pierson-Moskowitz spectrum $S^{1-\text{sided}}$ described in [55]:

$$S^{1-\text{sided}}(\omega) = \frac{5}{2\pi 16} H_s^2 T_p \left(\frac{\omega T_p}{2\pi}\right)^{-5} \exp\left[-\frac{5}{4}\left(\frac{\omega T_p}{2\pi}\right)^{-4}\right] \tag{3}$$

where $H_s$ is the significant wave height in m, defined as four times the standard deviation of sea elevation; $T_p$ is the peak spectral period of incident waves in s; and $\omega$ is the angular frequency of waves in rad/s.

Two types of waves have been considered: the most unfavourable and the least unfavourable. In the most unfavourable condition, the waves are completely sideways with an angle of 90° with respect to the direction of the mean wind speed and a $H_s = 2$ m, conditions used in [26]. The most favourable condition is when there are no lateral waves $H_s = 0$ m. Considering the oceanic meteorological environment of a generic U.S. east coast site, which is used in [47] for the analysis and design of the IEA Wind 15-MW reference turbine with fixed-bottom monopile support, an average $T_p$ value of 8 s was chosen.

For the optimization process of the AGTC controllers, stochastic turbulent winds generated with the NREL TurbSim tool were simulated [56] within region IV of the turbine operation. Specifically, three wind profiles have been designed with average wind speeds of 14, 18 and 22 m/s with a turbulence intensity of 14% and a vertical power-law shear with exponent 0.2 according to the Kaimal turbulence model defined by the Class B normal turbulence model in the IEC standard [57].

### B. CONTROL SYSTEM SCHEME

In this work, the wind turbine operates only in the rated region (region IV in Fig. 1), where the electromagnetic torque is set to its nominal value $T_{g,\text{rated}}$, and the pitch controller operates to maintain the nominal rotor speed.

The proposed control scheme, which is implemented using the Simulink software, is shown in Fig. 4. It consists of two controllers: a CPC and an AGTC. The control actions of these controllers generate the pitch $\beta_{\text{CPC}}$ and electromagnetic torque $T_g$ signals. According to (1), the generated power can be maintained at its rated value if the angular velocity of the wind turbine is controlled at its rated value $\omega_{g,\text{rated}}$. The CPC maintains this speed at its rated value, rejecting changes in wind speed $v_w$. To implement the CPC, we have used the Reference Open-Source Controller (ROSCO) and tuning parameters presented in [58].

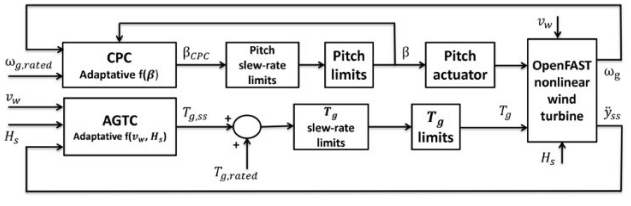


**FIGURE 4.** AGTC+CPC scheme for the full load region.

The controller to be designed in this work is the AGTC. Its main objective is to minimize the structural load of the tower lateral motion $y_{ss}$. To be more precise, the AGTC adds damping to the natural frequency of the lateral bending mode of the tower. The AGTC produces an additional component $T_{g,SS}$ of generator torque that is added to the nominal torque, as shown in (4). This additional component is proportional to the side-side velocity of the nacelle $\dot{y}_{SS}$. The final torque signal is constrained by considering the slew-rate and electromagnetic torque saturation limits. In most works, the extra component $T_{g,SS}$ is limited to ±10% of the nominal generator torque [27]. For direct-drive wind turbines (such as the IAE 15 MW turbine), the electrical torque on the generator is significantly higher compared to gear-driven wind turbines, which allows the tower lateral vibration to be damped more effectively by AGTC [26].

$$T_g = T_{g,\text{rated}} + T_{g,SS} = T_{g,\text{rated}} + k\dot{y}_{SS} \tag{4}$$

The specific AGTC scheme used in this work is shown in Fig. 5. The lateral velocity $\dot{y}_{SS}$ is calculated by integrating the lateral acceleration measured at the top of the tower. Such velocity is multiplied by the proportional gain $k$ to obtain the extra component $T_{g,SS}$. Variations in wind speed and significant wave height change the operating point of the turbine and consequently, the control is directly affected. Here, an adaptive control with scheduled gain of the AGTC using wind speed and wave height as scheduling variables is proposed to ensure proper performance for different wind and wave conditions.

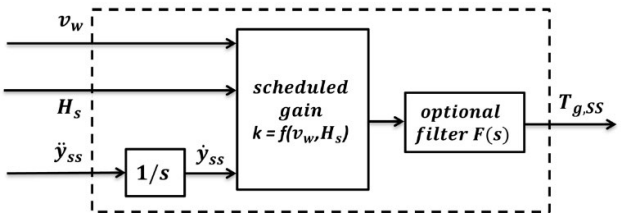


**FIGURE 5.** Adaptative AGTC scheme.

In addition, there is the option of including a second-order bandpass filter with the following transfer function:

$$F(s) = \frac{2\xi\omega_n s}{s^2 + 2\xi\omega_n s + \omega_n^2} \tag{5}$$

where $\omega_n = 2\pi f_n$ represents the first natural frequency of the tower in the lateral direction and $\xi$ characterizes the corresponding damping ratio. This filter limits the frequency band where AGTC should add active damping to avoid unnecessary actions in other frequency ranges.

To design the scheduled gain adaptive control of the AGTC with robustness to wind and wave changes, tuning of the controller is performed for the six operating points generated

by the combination of three wind conditions and two wave conditions described in the previous section.

From a control viewpoint, the model of Fig. 4 can be formulated by the system of nonlinear equations in (6), where state functions X(), constraint functions Z() and vector $\mathbf{x}$ and $\mathbf{z}$ are extended to include not only states and constraints of the OpenFAST wind turbine model in (2) but also the states and constraints of the control system in Simulink. The new input vector $\mathbf{u}$ is composed of the fixed rated rotational speed $\omega_g$, which is the CPC set point, the rated generator torque, which also remains fixed, the wind speed components $v_x$ and $v_y$, and the wave height $H_s$. The wind speed and wave height change during simulation and they work as disturbances. The new output function H() determines the output vector $\mathbf{y}$, which includes the variables of interest to analyse the performance of the system, such as the rotational speed, the nacelle lateral acceleration, the pitch control signal $\beta_{CPC}$, the electromagnetic torque $T_g$ signal, and different tower moments. All these variables depend on the AGTC parameter vector $\boldsymbol{\rho}$ to be tuned. The model also includes the inequations related to the saturation and slew-rate constraints on the control signals $\beta_{CPC}$ and $T_g$, which are implemented explicitly with Simulink blocks. The tuning of the AGTC block parameters is formulated as a multi-objective optimization problem described in the next section.

$$\begin{cases} \dot{\boldsymbol{x}} = \mathrm{X}\left(\boldsymbol{x}, \boldsymbol{z}, \boldsymbol{u}, t, \right) \\ 0 = \mathrm{Z}\left(\boldsymbol{x}, \boldsymbol{z}, \boldsymbol{u}, t, \right) \\ \boldsymbol{y} = \mathrm{H}\left(\boldsymbol{x}, \boldsymbol{z}, \boldsymbol{u}, t, \right) \\ 0 \leq \beta_{CPC}(\boldsymbol{x}, \boldsymbol{z}, \boldsymbol{u}, t, ) \leq \frac{1}{2} rad \\ \left|\dot{\beta}_{CPC}(\boldsymbol{x}, \boldsymbol{z}, \boldsymbol{u}, t, )\right| \leq 0.0349 \; rad/s \\ 17808 \leq T_g\left(\boldsymbol{x}, \boldsymbol{z}, \boldsymbol{u}, t, \right) \leq 21765 \; kNm \\ \left|\dot{T}_g(\boldsymbol{x}, \boldsymbol{z}, \boldsymbol{u}, t, )\right| \leq 4.5 \; MNm/s \end{cases} \tag{6}$$

### C. MULTI-OBJECTIVE OPTIMIZATION FORMULATION

In this section, the methodology for adjusting the AGTC block parameters is described. The main benefit of active vibration control using generator torque is the reduction of tower lateral oscillations and fatigue causing detrimental side effects, such as higher output power fluctuations and higher fatigue loads on drivetrain components, such as the main shaft [20]. The trade-off between energy efficiency and fatigue reduction in wind turbine control is approached in this paper as a MOO problem. This optimization problem is performed by proposing three objective functions to be minimized in the cost function vector J, as follows:

$$\mathbf{J} = \left[\mathrm{DEL}\left(\mathrm{M_{SS}}\right) \mathrm{DEL}\left(\mathrm{M_{LSS}}\right) \mathrm{TV}\left(\mathrm{P_g}\right)\right]^{\mathrm{T}} \tag{7}$$

The first two objective functions, $\mathrm{DEL}(M_{ss})$ and $\mathrm{DEL}(M_{LSS})$, are based on the fatigue damage equivalent load (DEL) and are chosen with the intention of minimizing the lateral fatigue load of the tower and the main rotating shaft through the tower lateral bending moment $M_{ss}$ and the moment on the low-speed shaft $M_{LSS}$, respectively. For fatigue assessment of wind turbines, the DEL is usually calculated in the time domain using cycle counting techniques. This function cannot be evaluated analytically since the DEL index is calculated offline from the time series of simulation data. The set of scripts MLife [59] is used to post-process the data from each simulation to obtain the corresponding DEL values.

The other cost objective function is the total variation in generated power $\mathrm{TV}(P_g)$ given in (8). It is employed to penalize control designs that result in significant fluctuations in the generated power. It is also calculated from the time series data after finishing a simulation with a total time $t_{sim}$ and discarding the initial $t_0$ seconds; derivatives and integrals are replaced by discrete numerical approximations.

$$\mathrm{TV}\left(\mathrm{P_g}\right) = \frac{1}{\mathrm{t_{sim}} - \mathrm{t_{sim}}} \int_{\mathrm{t_{sim}}}^{\mathrm{t_{sim}}} \left|\frac{\mathrm{dP_g}\left(t\right)}{\mathrm{d}t}\right| \mathrm{d}t \tag{8}$$

The proposed MOO problem can be formulated as shown in (9). The decision variables $\boldsymbol{\rho}$ match the tuning parameters of AGTC. In the case without filter (labelled as AGTC), the only parameter to be adjusted is the proportional gain, and the parameter vector is $\boldsymbol{\rho} = [k]$. In the case of using the bandpass filter (labelled as AGTC+F), the vector $\boldsymbol{\rho} = [k \; f_c \; \varepsilon]$. These design parameters are restricted to a solution space $S \in \mathbb{R}^1$ for AGTC or $S \in \mathbb{R}^3$ for AGTC+F. The three objective functions in (7), which depend on the tuning parameter vector $\boldsymbol{\rho}$, must be minimized subjected to the dynamical behaviour of the system defined by the equations in (6) and subjected to the solution space S.

$$\begin{aligned} &min\, DEL\left(M_{SS}(\boldsymbol{\rho})\right), min\, DEL\left(M_{LSS}(\boldsymbol{\rho})\right), min\, TV\left(P_g(\boldsymbol{\rho})\right) \\ &subject\ to\ \ (\boldsymbol{x}, \boldsymbol{z}, \boldsymbol{y})\ \ solution\ of\ \ (6) \\ &\qquad \boldsymbol{\rho} \in S \end{aligned} \tag{9}$$

This MOO problem is solved according to the procedure depicted in Fig. 6. This approach is based on calculating Pareto fronts and using decision makers to select the final satisfactory solution. Because the proposed objective functions in J are very complex, as well as the wind turbine dynamic

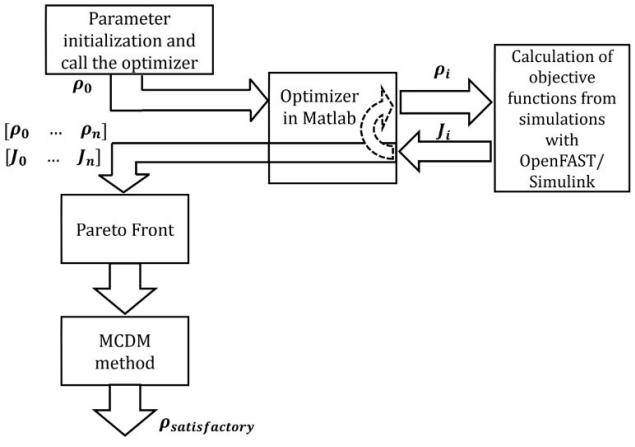


**FIGURE 6.** Multi-objective optimization procedure.

model, these cannot be evaluated analytically. Therefore, a simulation-based approach is applied to calculate Pareto front solutions using an optimizer, which needs to perform numerous co-simulations with OpenFAST and Simulink.

The AGTC parameter setting procedure is performed by simulating the IEA 15 MW wind turbine model around the six operating points already discussed by combining three wind speeds and two significant wave heights. The TOPSIS method is applied to each of the possible solutions for each Pareto front, and the best one according to this criterion is chosen as the best satisfactory solution. The tuning parameters connected to this solution are regarded as the optimal ones for that operating point. With them, the necessary parameters are obtained to build a lookup table of gains to implement the adaptive AGTC by scheduled gain.

### D. OPTIMIZATION ALGORITHM

The proposed optimization procedure becomes a nonlinear problem that requires great computational effort. To achieve better computational efficiency, the optimizer in Fig. 6 uses the nondominated sorting genetic algorithm-II (NSGA-II). Specifically, the NSGA-II algorithm used in this study is coded in the Global Optimization Toolbox of MATLAB. The NSGA-II algorithm consists of the following steps depicted in Fig. 7 [32]:

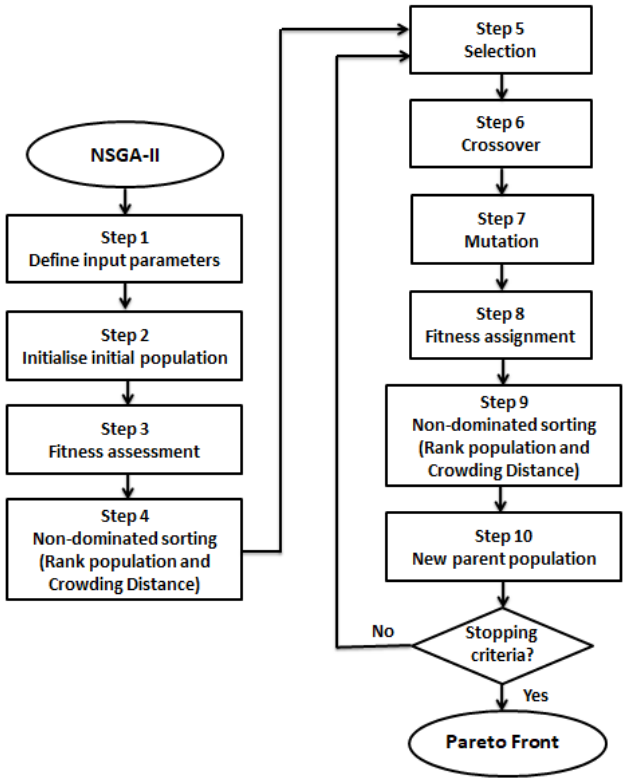


**FIGURE 7.** Procedure of NSGA-II.

1) Input parameter definition: the algorithm is configured by specifying parameters such as population size, stopping criteria, decision variable bounds, and objective functions. They are detailed in the next steps.
2) Initial population initialisation: prior to optimization, the search ranges of the tuning parameters are established manually using a bisection-like method in which the range is narrowed by discarding parameter values that result in instability in the simulation. The search range for gain $k$ is [0-10e8], the range for $f_c$ is [0.15-0.25] Hz and [0.001-20] for $\varepsilon$. An initial population of size 100 is created with equidistant parameter values within the set search range.
3) Fitness assessment: after the initialisation, the fitness values are assigned to each individual (or chromosome) in the population. The fitness functions are the cost functions in J to be optimized. In this proposed simulation-based approach, a simulation is performed for each individual to compute the corresponding fitness.
4) Non-dominated sorting: this method ranks the individuals in the population. Each solution is assigned a fitness (or rank) equal to its nondomination level (1 is the best, 2 is the next-best, and so on). Once the rank population is complete, the crowding distance, a measure of how many chromosomes there are in a particular chromosome's surrounding area, is assigned to each individual. Next, the steps to create an offspring population start.
5) Selection: the aim of this step is to choose the fittest individuals and let them pass their genes to the next generation. The selection function chooses parents based on their scaled values from the fitness functions. The scaled fitness values are called the expectation values. Once the individuals are sorted, the individuals are selected by using a binary tournament selection. This selection strategy randomly chooses a subset of individuals (or players) and then chooses the best individual from that set to be a parent. Individuals with a lower rank have a higher chance of selection. If individuals have the same nondomination rank, individuals with large crowding distance will be selected.
6) Crossover: this operator recombines the selected individuals (parents) two by two to create a fraction of the new population (children). It enables the algorithm to extract the best genes from different individuals and recombine them into potentially superior children. The crossover fraction configured in this work is 80% and indicates the fraction of population, other than elite children, that is created by crossover. The crossover operator chosen is the intermediate, which creates children by taking a weighted average of the parents.
7) Mutation: it makes small random changes in the individuals in the population, which provides genetic diversity and enable the genetic algorithm to search a broader space in order to avoid local optimum tracking, like crossover. The operator chosen is the adaptive feasible mutation, which randomly generates directions

that are adaptive with respect to the last successful or unsuccessful generation.

8) Fitness assessment: the objective functions are evaluated with the new offspring population.
9) Non-dominated sorting: non-dominated solutions from combined population (parent population + offspring population) are sorted similarly to step 4.
10) New parent population: individuals are replaced with the best ones for the next generation.

Then, the process repeats steps from 5 to 10 until the stopping criteria is met. In this work, when the number of generations reaches 50, the process stops and outputs a non-dominant Pareto front. As the Pareto front population fraction was set to 25%, the resultant Pareto front is composed of 25 nondominated solutions. The computational time to run the proposed optimization procedure is in the order of tens of hours, which is in line with what is reported in [41] for problems with three objective functions based on a simulation approach using OpenFAST.

### E. RESULTANT PARETO FRONTS

Figure 8 shows the 3D Pareto fronts for the six operating points analysed in this work, both for the scheme AGTC without filter (in red) and for the scheme AGTC+F with filter (in blue). The fronts in the left column have been calculated with the presence of side waves and those on the right without side waves. The fronts in each row are associated with wind profiles of 22, 18 and 14 m/s, respectively. In each front, the best solution according to TOPSIS method is highlighted with a diamond.

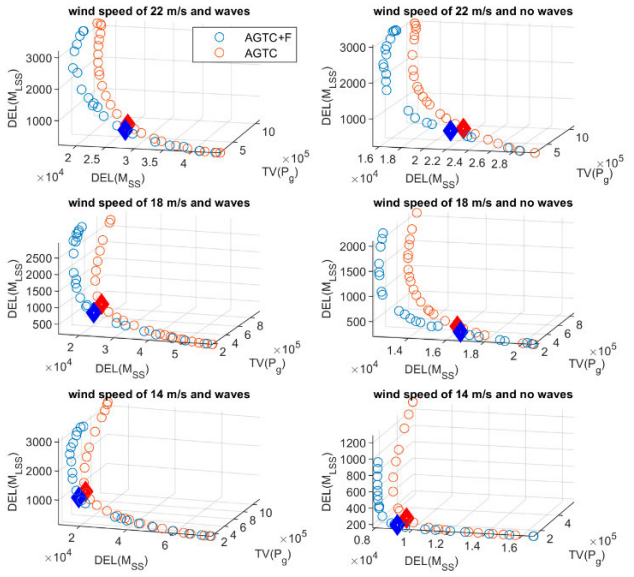


**FIGURE 8.** 3D Pareto fronts for AGTC and AGTC+F obtained with different conditions of wind and waves.

Simulations during the optimization process are performed with a total time of 800 s; however, the first 200 s are discarded to exclude transient effects on the data. The sampling frequency was set to 200 Hz. Tables 2 and 3 show the objective functions and optimal parameters in both AGTC schemes, respectively, for the six weather conditions. Table 3 also includes, in parentheses, the values of the objective functions in percentages with respect to the AGTC without filter.

**TABLE 2.** Optimal AGTC parameters and objective indices.

| Wind speed (m/s) | DEL($M_{SS}$) (kNm) | DEL($M_{LSS}$) (kNm) | TV($P_g$) (kW) | $k$ (Ns) |
|---|---|---|---|---|
| 22 | 2.3227e4 | 764.5054 | 2.9188e5 | 3.6096e6 |
| 18 | 1.6428e4 | 435.2975 | 2.3410e5 | 2.7641e6 |
| 14 | 9.5293e3 | 269.1525 | 1.5748e5 | 2.2463e6 |
| 22 +waves | 2.8197e4 | 878.4606 | 2.9954e5 | 3.7313e6 |
| 18 +waves | 2.4071e4 | 1.0056e3 | 3.1379e5 | 5.1379e6 |
| 14 +waves | 1.9155e4 | 1.1491e3 | 2.8603e5 | 7.0434e6 |

**TABLE 3.** Optimal AGTC+F parameters and objective indices.

| Wind speed (m/s) | DEL($M_{SS}$) (kNm) | DEL($M_{LSS}$) (kNm) | TV($P_g$) (kW) | $k$ (Ns) | $f_c$ (Hz) | $\xi$ |
|---|---|---|---|---|---|---|
| 22 | 2.2358e4 (-3.74%) | 752.0980 (-1.62%) | 2.1722e5 (-25.6%) | 4.9150e6 | 0.1727 | 0.3492 |
| 18 | 1.6751e4 (+1.96%) | 374.7308 (-13.91%) | 1.8222e5 (-22.2%) | 3.5058e6 | 0.1717 | 0.3652 |
| 14 | 9.1974e3 (-3.48%) | 210.3921 (-21.83%) | 1.2617e5 (-19.9%) | 3.2171e6 | 0.1707 | 0.3393 |
| 22 +waves | 2.8366e4 (+0.59%) | 790.0034 (-10.06%) | 2.2159e5 (-26.0%) | 4.7519e6 | 0.1719 | 0.3065 |
| 18 +waves | 2.3971e4 (-0.41%) | 896.5749 (-10.84%) | 1.9664e5 (-37.3%) | 5.8929e6 | 0.1711 | 0.3271 |
| 14 +waves | 1.8879e4 (-1.44%) | 1.1021e3 (-4.09%) | 1.5913e5 (-44.4%) | 7.7758e6 | 0.1720 | 0.4893 |

The use of the bandpass filter in AGTC+F achieves optimal points with significant reduction in TV($P_g$) and improvement in DEL($M_{LSS}$), maintaining similar values in DEL($M_{SS}$). This is also seen in the 2D projections of the Pareto fronts, as shown in Fig. 9 for the operating point with wind of 18 m/s with waves, where the TV($P_g$)-DEL($M_{SS}$) projection corresponding to the AGTC+F scheme is more displaced to the left than that of the AGTC scheme.

The gain $k$ values of the AGTC+F are higher, which allows more focus on damping the lateral momentum of the $M_{SS}$ tower at frequency $f_c$. For the design of the AGTC+F adaptive control, frequency $f_c$ has been set at 0.172 Hz and $\xi$ at 0.4 as average values from Table 3 since they show very little variation between operating points.

As for the gain $k$, the proposed AGTC schemes are designed to address all possible operating points within the nominal region. To cover all this operating range, a linear interpolation of the gain $k$ of the AGTC schemes as a function of wind speed $v_w$ and wave height $H_s$ was performed. The meshing performed is for a range of wind speeds from 14 to 22 m/s in 0.5 m/s intervals and wave height values from 0 to 2 m in 0.2 m intervals. The surfaces obtained for the gain $k$ as

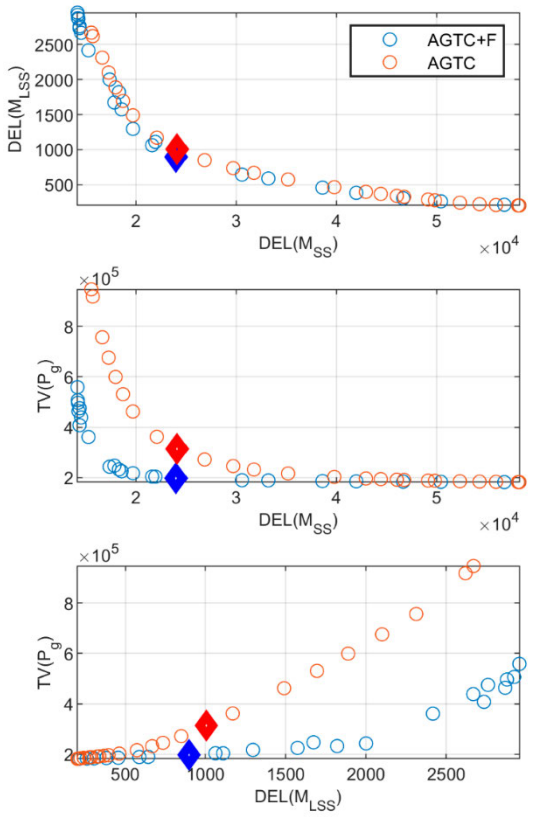


**FIGURE 9.** 2D projections of the Pareto fronts obtained for conditions with wind speed of 18 m/s and waves.

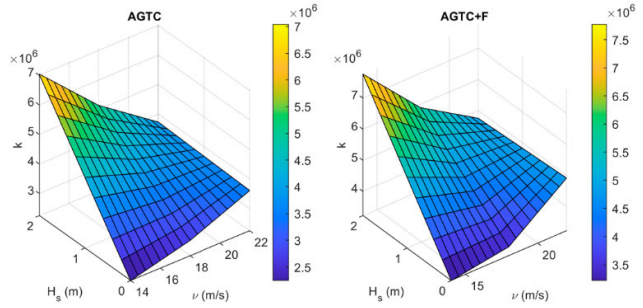


**FIGURE 10.** Interpolated surfaces for scheduled gain k of the AGTC schemes in function of the wind speed and lateral wave height.

a function of $\nu_w$ and $H_s$ for both AGTC schemes are shown in Fig. 10. The adaptive AGTC scheme continuously varies $k$ by interpolating between points within these 3D surfaces.

## IV. EVALUATION OF PROPOSED CONTROLLERS

In this section, the performance of the two AGTC schemes designed in the previous section for the IEA 15 MW wind turbine is evaluated using two simulations with different environmental conditions: case 1 that does not incorporate waves and case 2 that does simulate waves. Both cases use stochastic turbulent wind with varying wind speed ranges within the full load region. The wind profile was generated with TurbSim according to the IEC 61400-1 standard. The simulations have a total time of 1200 s, eliminating the first 200 seconds to exclude transient effects in the data. The sampling frequency was set to 200 Hz. In case 2, which is the most unfavourable case, the turbine is also subjected to irregular lateral waves following the JONSWAP/Pierson-Moskowitz spectrum. Different environmental conditions are analysed to study how generalizable the optimization results are, the robustness of the proposed controllers, and the influence of wind and wave conditions.

From the data obtained for each control strategy, an analysis of the most relevant variables in the time and frequency domains was performed. In addition, for each control strategy, different performance indices related to the fatigue suffered in the most essential components of the turbine, the generated power, the generator speed, the pitch signal, or the electromagnetic torque were quantified. In the comparative analysis, the ROSCO CPC, which does not incorporate AGTC, was used as the baseline control.

### A. CASE 1: SIMULATION WITHOUT WAVES

Figures 11 and 12 show the time response of the control strategies to be compared for case 1. Figure 11 shows the variables related to the CPC and Figure 12 the variables most related to the AGTC. Table 4 collects the rate of variation (TV) and standard deviation (STD) of some of the variables in these figures as performance indices for quantitative analysis.

From top to bottom, Figure 11 shows the frontal and lateral components of wind speed, generated power, generator angular velocity and collective blade pitch. Qualitatively, no significant differences in these wind turbine variables are apparent, indicating that the performance in the CPC loop is not affected by the additional AGTC scheme, as was expected. This is also quantitatively corroborated by the TV and STD data for both pitch and generator speed in Table 4, as there are no significant differences between the different control schemes. Figure 12 shows the variables most related to the AGTC loop, specifically, from top to bottom: the lateral moment at the base of the tower, the tower lateral displacements, the torque on the low-speed axis, the manipulated electromagnetic torque, and the adaptive proportional gain $k$ of the AGTC schemes. Compared to the reference CPC control, the AGTC schemes manage to significantly reduce the fluctuations in the lateral displacements at the top of the tower $y_{ss}$ and the lateral moments at the base of the tower in exchange for a worsening in the torsional moment on the low-speed shaft. This is also quantitatively confirmed by the performance indices in Table 4, in particular by the reduction achieved by the AGTC schemes in the TV and STD values of the tower lateral displacements and tower lateral moment at the cost of increased electromagnetic torque activity. If we compare the two AGTC schemes in the zoom of the graph, it is observed how AGTC+F smooths the electromagnetic torque response compared to AGTC without filter. According to the data in Table 4, the use of filter in AGTC+F reduces by 73.51% the TV of the electromagnetic torque with respect

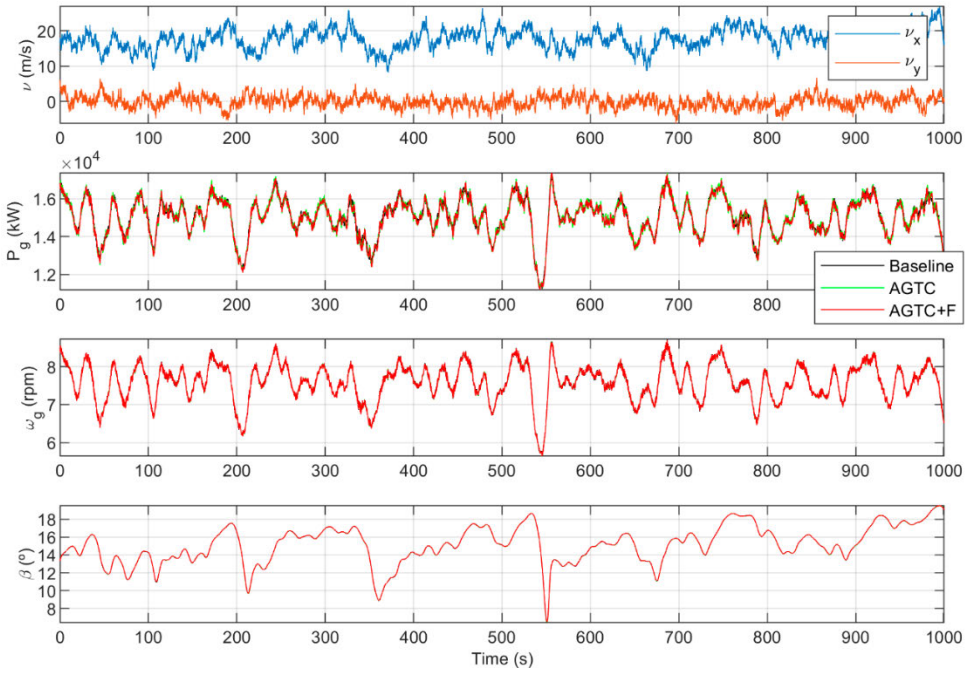


**FIGURE 11.** Time response of wind speed ($\nu$), generated power ($P_g$), angular velocity ($\omega_g$), and pitch ($\beta$) for case 1 (no waves).

to AGTC without filter, obtaining even slightly lower values of STD for torque $M_{ss}$, and displacements $y_{ss}$.

Table 5 shows the three indices used as objective functions in the MOO and calculated with the simulation data of case 1. The use of AGTC reduces the DEL($M_{ss}$) at the cost of worsening mainly the DEL($M_{LSS}$) and little the TV($P_g$). In absolute terms (kNm), the AGTC schemes manage to decrease the DEL($M_{ss}$) much more (around 20000 kNm) than to increase the DEL($M_{LSS}$). The DEL of the low-speed shaft torque $M_{LSS}$ only increases around 450 kNm; this increase is produced by the action of the AGTC on the electromagnetic torque. If we compare both AGTC schemes with each other, the AGTC+F achieves more reduction in $M_{ss}$ fatigue with less increase in $M_{LSS}$ fatigue than the AGTC without filter. The AGTC+F achieves more than 5% reduction in DEL($M_{LSS}$) compared to the AGTC controller without filter. In addition, AGTC+F achieves a similar TV($P_g$) value as the reference CPC control. The latter is consistent with the lower TV($T_g$) achieved by AGTC+F. In summary, AGTC+F achieves the best compromise between the three objectives.

Even though this work focuses on the study and reduction of the tower lateral loads and their engagement with the low-speed shaft moments, the DELs of other important loads of a wind turbine such as the fore-aft moments of the tower base or the flapwise and edgewise moments of the blades have been calculated. Although these values are not shown, the DELs related to these three moments are practically the same for all three control schemes analysed, indicating that the AGTC does not have a significant effect on these loads.

**TABLE 4.** Performance indices for case 1.

| Control system | Baseline | AGTC | AGTC+F |
|---|---|---|---|
| TV(β) (°) | 150.12 | 149.62 | 149.35 |
| STD(β) (°) | 2.07 | 2.07 | 2.07 |
| TV($\omega_g$) (rpm) | 350.22 | 346.72 | 350.25 |
| STD($\omega_g$) (rpm) | 0.47 | 0.47 | 0.47 |
| TV($T_g$) (kNm) | 0 | 6.40E+05 | 1.69E+05 |
| STD($T_g$) (kNm) | 0 | 184.43 | 183.87 |
| STD($M_{SS}$) (kNm) | 25378 | 13287 | 13144 |
| STD($y_{SS}$) (m) | 0.0638 | 0.0408 | 0.0393 |

**TABLE 5.** Cost functions used in the MOO calculated with the simulation data of case 1.

| Control system | Baseline | AGTC | AGTC+F |
|---|---|---|---|
| DEL($M_{SS}$) (kNm) | 48814 | 29228 (-19586) | 27949 (-20865) |
| DEL($M_{LSS}$) (kNm) | 305.31 | 788.51 (+483.2) | 748.02 (+442.7) |
| TV($P_g$) (kW) | 6.95e5 | 9.17e5 | 7.04e5 |

Figure 13 shows the Fourier amplitude spectrum obtained by Fast Fourier Transformation (FFT) of the side-side tower bending moment, generated electric power, low-speed shaft torsion moment, and generator torque for case 1 (simulation without waves). With respect to the side-side tower bending moment, the first mode is appreciated at around 0.175 Hz.

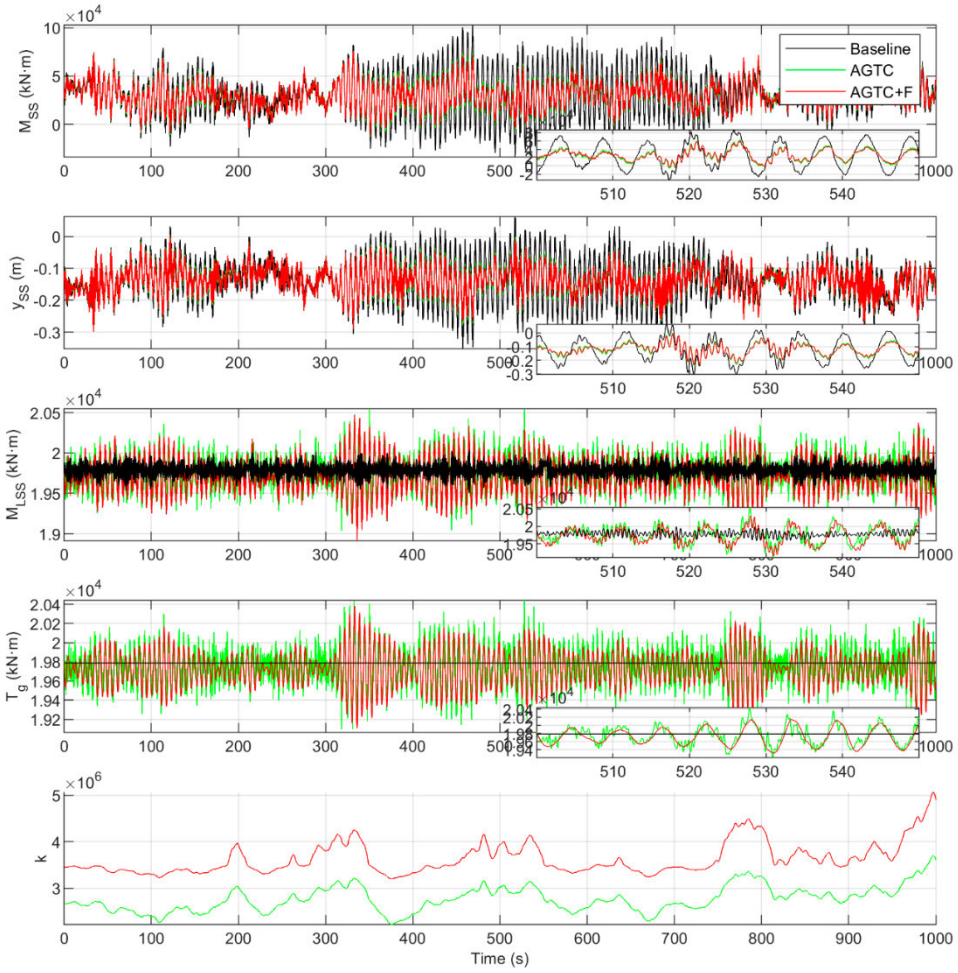


**FIGURE 12.** Time responses of lateral moment at tower base ($M_{SS}$), tower lateral displacement ($y_{SS}$), torque moment at low-speed axis ($M_{LSS}$), electromagnetic torque ($T_g$), and adaptive gain of AGTC (k) for case 1 (without waves).

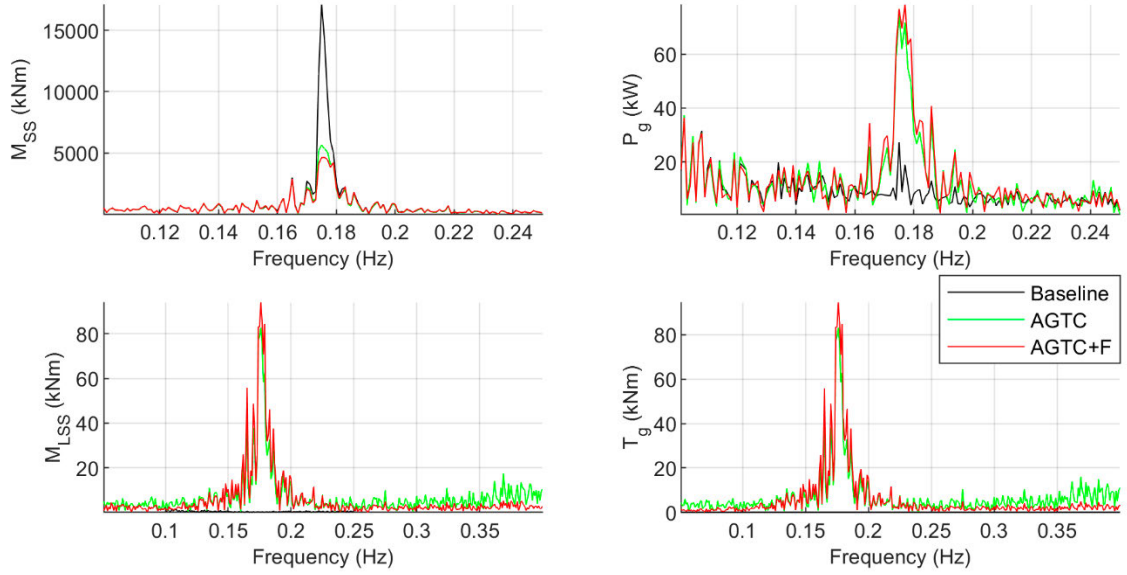


**FIGURE 13.** Fourier amplitude spectrum of the lateral moment at tower base ($M_{SS}$), generated power ($P_g$), torque moment at low-speed axis ($M_{LSS}$), and electromagnetic torque ($T_g$) for case 1 (without waves).

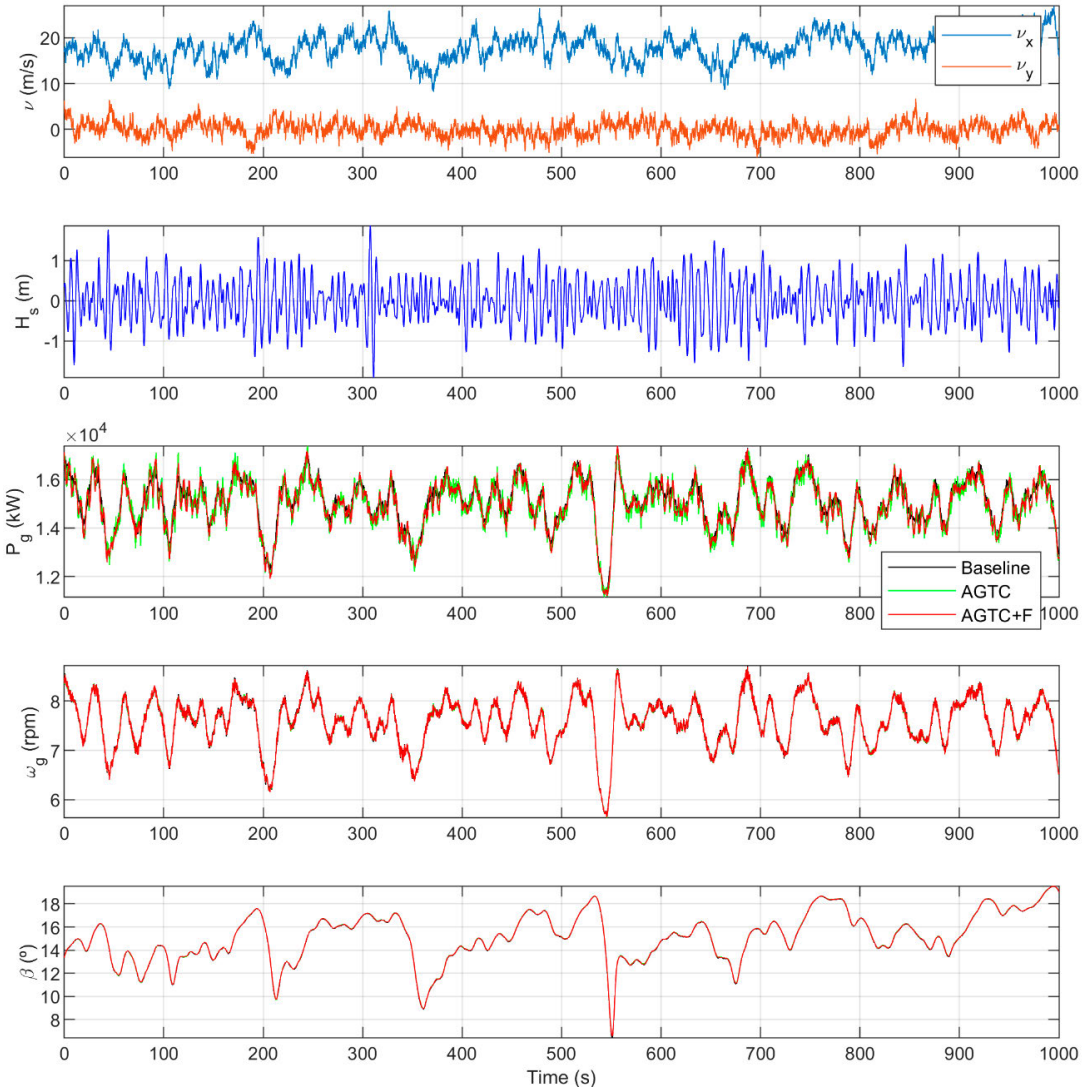


**FIGURE 14.** Time response of wind speed ($v$), wave height ($H_S$), generated power ($P_g$), angular velocity ($\omega_g$), and pitch ($\beta$) for case 2 (with waves).

The AGTC schemes obtain a significantly lower peak than the baseline control. If we compare both AGTC schemes, this peak is reduced somewhat more by the scheme with filter. With respect to the variables $P_g$, $M_{LSS}$ and $T_g$, the use of AGTC adds additional activity in part of the frequency range, in addition to a peak around 0.175 Hz.

If we compare both AGTC schemes, this peak is slightly higher for AGTC+F as the filter makes the torque stress more focused on the natural frequency of the lateral vibration of the tower, but thanks to this it reduces the activity at the other frequencies. This frequency analysis is in accordance with the results of the comparative analysis in the time domain.

### B. CASE 2: SIMULATION WITH WAVES

In this second case, in addition to the stochastic wind profile, a simulation is performed with irregular waves following the JONSWAP/Pierson-Moskowitz spectrum and impinging on the tower perpendicular to the wind, which makes the control task more difficult because they represent significant disturbances on the system. A study similar to that of case 1 is conducted. Figures 14 and 15 show the time response of the control strategies to be compared for case 2. Figure 14 shows the variables most related to CPC and Figure 15 the variables most related to AGTC. Table 6 shows the TV and STD of some variables analysed as performance indices for a quantitative analysis.

From top to bottom, Figure 14 shows the frontal and lateral components of wind speed, wave height profile, generated power, generator angular velocity, and collective blade pitch. As in case 1, qualitatively no significant differences in these wind turbine variables associated with the CPC loop are apparent, which does not seem to be affected by the additional AGTC scheme. This is also corroborated quantitatively with the TV and STD data for both pitch and generator speed

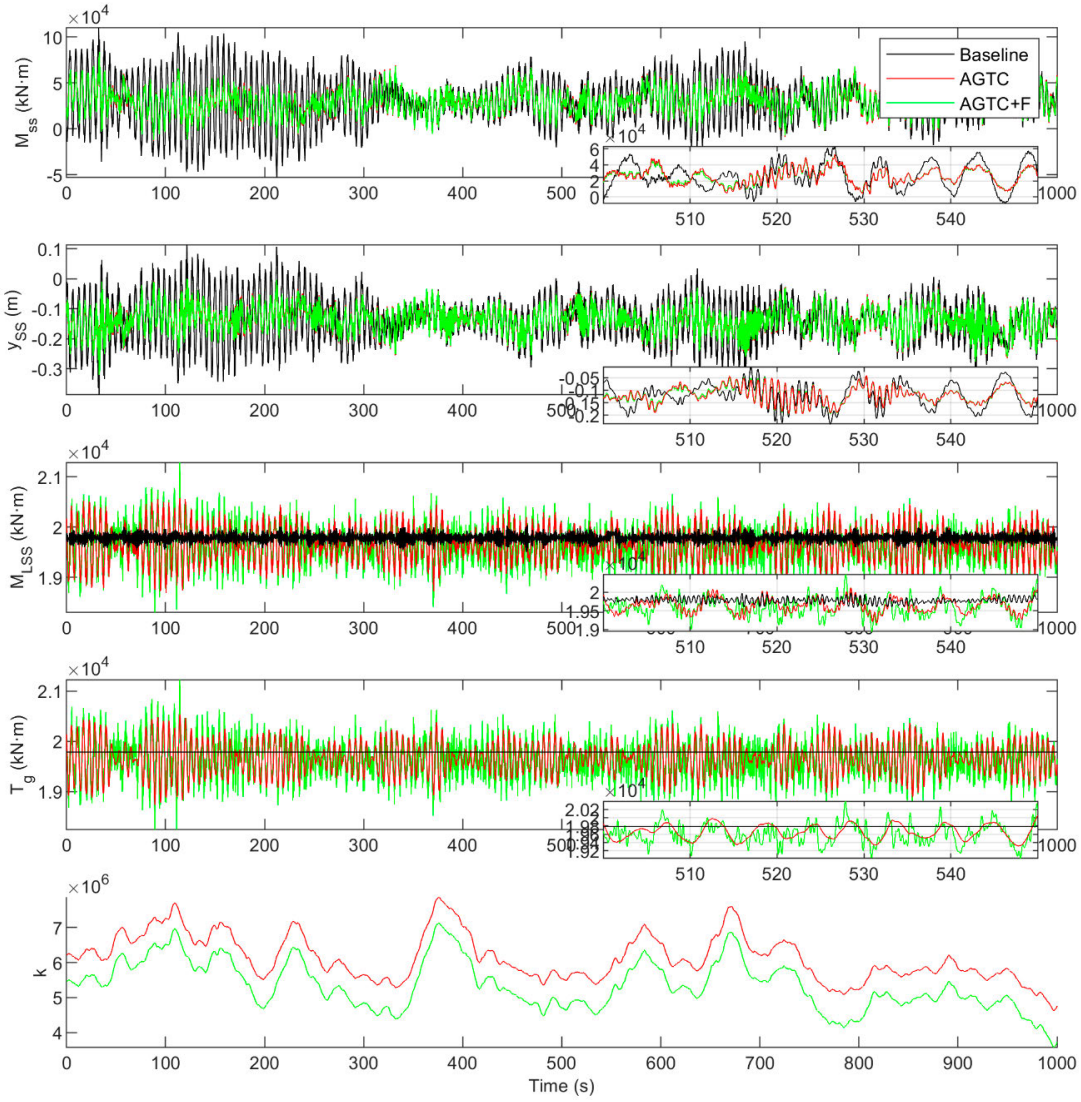


**FIGURE 15.** Time response of lateral moment at tower base ($M_{SS}$), tower lateral displacement ($y_{SS}$), torque moment at low-speed axis ($M_{LSS}$), electromagnetic torque ($T_g$), and adaptive gain of AGTC (k) for case 2 (with waves).

in Table 6, as there are no significant differences between the different control schemes. Only the generated power is somewhat worsened with the unfiltered AGTC because its higher activity in the electromagnetic torque produces more variations in the generated power.

Figure 15 shows the variables most related to the AGTC loop, from top to bottom: the lateral moment at the tower base, the tower lateral displacements, the torque on the low-speed axis, the manipulated electromagnetic torque, and the adaptive proportional gain $k$ of the AGTC schemes. As in case 1, the AGTC schemes contribute to reducing the fluctuations in the tower lateral displacements and their lateral moments in exchange for a worsening in the torsional moment on the low-speed shaft. The same is indicated by the performance indices in Table 6, specifically with the reduction achieved by the AGTC schemes in the TV and STD values of the tower lateral displacement and lateral moment at the cost of the increase in the rate of variation of the electromagnetic torque. If we compare the two AGTC schemes, zooming in the graph, it is again observed how AGTC+F smooths the electromagnetic torque response compared to AGTC without filter. According to the data in Table 6, AGTC+F reduces by 76.34% the TV of the electromagnetic torque with respect to AGTC without filter, obtaining even slightly lower STD values for torque, $M_{ss}$, and $y_{ss}$.

As in case 1, if we analyse the indices used in the MOO, the AGTC+F control again achieves the best compromise between DEL($M_{ss}$), DEL($M_{LSS}$) and TV($P_g$), as shown by the data in Table 7. The use of AGTC reduces tower lateral fatigue at the cost of worsening mainly shaft fatigue. But as in case 1, in absolute terms this increase in DEL($M_{LSS}$) of about 750-1100 kNm is much smaller than the reduction achieved in DEL($M_{ss}$) of about 27000 kNm. The use of a filter in the AGTC+F achieves more than 24% reduction in

**TABLE 6. Performance indices for case 2.**

| Control system | Baseline | AGTC | AGTC+F |
|---|---|---|---|
| TV(β) (º) | 150.03 | 153.03 | 148.98 |
| STD(β) (º) | 2.078 | 2.074 | 2.072 |
| TV($\omega_g$) (rpm) | 350.91 | 349.27 | 350.79 |
| STD($\omega_g$) (rpm) | 0.477 | 0.478 | 0.477 |
| TV($T_g$) (kNm) | 0 | 1.23E+06 | 2.91E+05 |
| STD($T_g$) (kNm) | 0 | 345.02 | 309.97 |
| STD($M_{SS}$) (kNm) | 22461 | 13502 | 12912 |
| STD($y_{SS}$) (m) | 0.0715 | 0.0402 | 0.0401 |

**TABLE 7. Cost functions used in the MOO calculated with the simulation data of case 2.**

| Control system | Baseline | AGTC | AGTC+F |
|---|---|---|---|
| DEL($M_{SS}$) (kNm) | 55868 | 28819 (-27049) | 28901 (-26967) |
| DEL($M_{LSS}$) (kNm) | 304.33 | 1388.2 (+1083.9) | 1052.3 (+747.97) |
| TV($P_g$) (kW) | 6.96e5 | 12.52e5 | 7.26e5 |

the DEL($M_{LSS}$) compared to the AGTC scheme without filter and obtains a TV($P_g$) similar to that of the baseline control without AGTC.

Moreover, as in case 1, the AGTC schemes do not affect the DELs of the other main turbine moments. The frequency response results are also similar to those in case 1.

## V. CONCLUSION

This paper proposes a control strategy for the reduction of tower side loads of large-scale variable speed-variable pitch horizontal axis wind turbines working in their nominal region of operation. The control scheme combines two controllers: a collective pitch control (CPC) that regulates the turbine speed and an active electromagnetic torque control (AGTC) that adds an additional component to the nominal torque set to mitigate the lateral fatigue suffered in the tower. This work focuses on the design of the latter AGTC controller while using a previously designed CPC. Two AGTC configurations are proposed: a proportional control and a proportional control with filter. They are implemented as adaptive controllers by scheduled gain at different operating points as a function of wind speed and wave height. The AGTC parameter tuning procedure is formulated as a multi-objective optimization problem for several operating points. This is solved by means of genetic algorithms to obtain Pareto front solutions where three objective functions are considered: two related to the fatigue load suffered by the wind turbine, such as the DEL of the lateral moment at the base of the tower and the DEL of the moment at the low-speed axis, and another objective related to the fluctuations of the generated power, such as its variation rate. At each front, the TOPSIS method is used as MCDM to decide the satisfactory compromise solution between these objectives, which determines the optimal parameters of the AGTC at that point. The optimization procedure is performed based on simulations conducted with MATLAB/Simulink to implement the controllers along with OpenFAST to simulate the turbine in different wind and wave conditions in the nominal region.

The proposed method has been applied to an IAE 15MW offshore wind turbine with a monopile structure; the designed controllers have been evaluated in two scenarios with different wind-wave conditions and compared with the ROSCO controller without AGTC as baseline control. The simulation results show a good compromise between different objectives, which is one of the main advantages of the proposed methodology. In other studies, the AGTCs obtained better structural performance in the lateral moments of the tower at the cost of a worsening in the quality of generated power and/or shaft moments. However, with the proposed methodology, AGTCs obtain acceptable results for the generated power quality while maintaining a significant reduction in tower lateral fatigue loading, at the cost of a worsening, compared to the non-AGTC control, of the shaft moments caused by the AGTCs use of electromagnetic torque. The AGTC with filter achieves the best balance between the three objectives since, compared to the AGTC without filter, it does not increase the shaft moment DEL as much because the filter attenuates the electromagnetic torque action.

Although the methodology has been applied to a 15 MW wind turbine, it could be used on all types of large-scale horizontal axis wind turbines and variable speed-variable pitch turbines, onshore or offshore, with monopile structures or floating platforms.

## ACKNOWLEDGMENT

The authors would like to thank CENER for their collaboration and valuable contributions.

## REFERENCES

[1] European Commission. *The Commission Calls for a Climate Neutral Europe by 2050*. Accessed: Apr. 24, 2023. [Online]. Available: https://ec.europa.eu/commission/presscorner/detail/en/IP_18_6543

[2] J. López-Queija, E. Robles, J. Jugo, and S. Alonso-Quesada, "Review of control technologies for floating offshore wind turbines," *Renew. Sustain. Energy Rev.*, vol. 167, Oct. 2022, Art. no. 112787, doi: 10.1016/j.rser.2022.112787.

[3] H. Zuo, K. Bi, and H. Hao, "A state-of-the-art review on the vibration mitigation of wind turbines," *Renew. Sustain. Energy Rev.*, vol. 121, Apr. 2020, Art. no. 109710, doi: 10.1016/j.rser.2020.109710.

[4] J. G. Njiri and D. Söffker, "State-of-the-art in wind turbine control: Trends and challenges," *Renew. Sustain. Energy Rev.*, vol. 60, pp. 377–393, Jul. 2016, doi: 10.1016/j.rser.2016.01.110.

[5] E. J. N. Menezes, A. M. Araújo, and N. S. B. da Silva, "A review on wind turbine control and its associated methods," *J. Cleaner Prod.*, vol. 174, pp. 945–953, Feb. 2018, doi: 10.1016/j.jclepro.2017.10.297.

[6] J. E. Sierra-Garcia, M. Santos, and R. Pandit, "Wind turbine pitch reinforcement learning control improved by PID regulator and learning observer," *Eng. Appl. Artif. Intell.*, vol. 111, May 2022, Art. no. 104769, doi: 10.1016/j.engappai.2022.104769.

[7] J. E. Sierra-Garcia and M. Santos, "Deep learning and fuzzy logic to implement a hybrid wind turbine pitch control," *Neural Comput. Appl.*, vol. 34, no. 13, pp. 10503–10517, Jul. 2022

[8] N. T. Vu, H. D. Nguyen, and A. T. Nguyen, "Reinforcement learning-based adaptive optimal fuzzy MPPT control for variable speed wind turbine," *IEEE Access*, vol. 10, pp. 95771–95780, 2022, doi: 10.1109/ACCESS.2022.3205124.

[9] M. Patrascu and A. Ion, "Evolutionary modeling of industrial plants and design of PID controllers," in *Nature-Inspired Computing for Control Systems* (Studies in Systems, Decision and Control), vol. 40. Cham, Switzerland: Springer, 2016, pp. 73–119, doi: 10.1007/978-3-319-26230-7_4.

[10] J. E. Sierra-García and M. Santos, "Performance analysis of a wind turbine pitch neurocontroller with unsupervised learning," *Complexity*, vol. 2020, pp. 1–15, Sep. 2020, doi: 10.1155/2020/4681767.

[11] J. E. Sierra-García and M. Santos, "Improving wind turbine pitch control by effective wind neuro-estimators," *IEEE Access*, vol. 9, pp. 10413–10425, 2021, doi: 10.1109/ACCESS.2021.3051063.

[12] G. Malliotakis, P. Alevras, and C. Baniotopoulos, "Recent advances in vibration control methods for wind turbine towers," *Energies*, vol. 14, no. 22, p. 7536, Nov. 2021, doi: 10.3390/en14227536.

[13] S. Sarkar and B. Fitzgerald, "Vibration control of spar-type floating offshore wind turbine towers using a tuned mass-damper-inerter," *Struct. Control Health Monitor.*, vol. 27, no. 1, Jan. 2020, Art. no. e2471, doi: 10.1002/stc.2471.

[14] P. Alkhoury, M. Aít-Ahmed, A.-H. Soubra, and V. Rey, "Vibration reduction of monopile-supported offshore wind turbines based on finite element structural analysis and active control," *Ocean Eng.*, vol. 263, Nov. 2022, Art. no. 112234, doi: 10.1016/j.oceaneng.2022.112234.

[15] E. Smilden, E. E. Bachynski, A. J. Sørensen, and J. Amdahl, "Wave disturbance rejection for monopile offshore wind turbines," *Wind Energy*, vol. 22, no. 1, pp. 89–108, Jan. 2019, doi: 10.1002/we.2273.

[16] Y. Liu, S. Zhang, X. Wang, H. Xie, and T. Cao, "Optimization of pitch control parameters for a wind turbine based on tower active damping control," *Energies*, vol. 15, no. 22, p. 8686, Nov. 2022, doi: 10.3390/en15228686.

[17] C. Serrano, J.-E. Sierra-Garcia, and M. Santos, "Hybrid optimized fuzzy pitch controller of a floating wind turbine with fatigue analysis," *J. Mar. Sci. Eng.*, vol. 10, no. 11, p. 1769, Nov. 2022, doi: 10.3390/jmse10111769.

[18] A. Gambier and Y. Y. Nazaruddin, "Wind turbine pitch and active tower damping control using metaheuristic multi-objective bat optimization," in *Proc. 21st Int. Conf. Modeling Appl. Simulation (MAS)*, 2022, pp. 1–9, doi: 10.46354/I3M.2022.MAS.025.

[19] B. Fischer and M. Shan, "A survey on control methods for the mitigation of tower loads," Fraunhofer-IWES, Bremerhaven, Germany, Tech. Rep. 655, 2013, Accessed: Apr. 24, 2023. [Online]. Available: https://publica.fraunhofer.de/bitstreams/f0c70706-6842-454d-a14f-4fa050f7787a/download

[20] T. Fischer, P. Rainey, E. Bossanyi, and M. Kühn, "Study on control concepts suitable for mitigation of loads from misaligned wind and waves on offshore wind turbines supported on monopiles," *Wind Eng.*, vol. 35, no. 5, pp. 561–573, Oct. 2011, doi: 10.1260/0309-524x.35.5.561.

[21] T. Fischer, W. De Vries, and B. Schmidt, "UpWind Design Basis (WP4: Offshore foundations and support structures)," Inst. Aircr. Des. Universität Stuttgarrt, Germany, Tech. Rep., 2010, Accessed: Apr. 24, 2023. [Online]. Available: http://resolver.tudelft.nl/uuid:a176334d-6391-4821-8c5f-9c91b6b32a27

[22] X. Liu, J. Xu, G. He, and C. Chen, "Lateral vibration mitigation of monopile offshore wind turbines with a spring pendulum pounding tuned mass damper," *Ocean Eng.*, vol. 266, Dec. 2022, Art. no. 112954, doi: 10.1016/j.oceaneng.2022.112954.

[23] Z. Zhang, A. Staino, B. Basu, and S. R. K. Nielsen, "Performance evaluation of full-scale tuned liquid dampers (TLDs) for vibration control of large wind turbines using real-time hybrid testing," *Eng. Struct.*, vol. 126, pp. 417–431, Nov. 2016, doi: 10.1016/j.engstruct.2016.07.008.

[24] A. F. Mensah and L. Dueñas-Osorio, "Improved reliability of wind turbine towers with tuned liquid column dampers (TLCDs)," *Struct. Saf.*, vol. 47, pp. 78–86, Mar. 2014, doi: 10.1016/j.strusafe.2013.08.004.

[25] E. Smilden, E. E. Bachynski, A. J. Sørensen, and J. Amdahl, "Site-specific controller design for monopile offshore wind turbines," *Mar. Struct.*, vol. 61, pp. 503–523, Sep. 2018, doi: 10.1016/j.marstruc.2018.03.002.

[26] Z. Zhang, S. Nielsen, F. Blaabjerg, and D. Zhou, "Dynamics and control of lateral tower vibrations in offshore wind turbines by means of active generator torque," *Energies*, vol. 7, no. 11, pp. 7746–7772, Nov. 2014, doi: 10.3390/en7117746.

[27] F. Golnary and K. T. Tse, "Simultaneous active control of tower lateral vibration and power control of wind turbine: A novel multivariable approach," *Energy Rep.*, vol. 8, pp. 4233–4251, Nov. 2022, doi: 10.1016/j.egyr.2022.03.083.

[28] P. F. Odgaard, L. F. S. Larsen, R. Wisniewski, and T. G. Hovgaard, "On using Pareto optimality to tune a linear model predictive controller for wind turbines," *Renew. Energy*, vol. 87, pp. 884–891, Mar. 2016, doi: 10.1016/j.renene.2015.09.067.

[29] Y. Cui, Z. Geng, Q. Zhu, and Y. Han, "Review: Multi-objective optimization methods and application in energy saving," *Proc. Energy*, vol. 125, pp. 681–704, Apr. 2017, doi: 10.1016/j.energy.2017.02.174.

[30] D. Fogel, "The advantages of evolutionary computation," in *Biocomputing and Emergent Computation*. Singapore: World Scientific, 1997, pp. 1–11, doi: 10.1142/3593.

[31] G. Chiandussi, M. Codegone, S. Ferrero, and F. E. Varesio, "Comparison of multi-objective optimization methodologies for engineering applications," *Comput. Math. With Appl.*, vol. 63, no. 5, pp. 912–942, Mar. 2012, doi: 10.1016/j.camwa.2011.11.057.

[32] K. Deb, A. Pratap, S. Agarwal, and T. Meyarivan, "A fast and elitist multiobjective genetic algorithm: NSGA-II," *IEEE Trans. Evol. Comput.*, vol. 6, no. 2, pp. 182–197, Apr. 2002, doi: 10.1109/4235.996017.

[33] M. Lara, J. Garrido, M. L. Ruz, and F. Vázquez, "Multi-objective optimization for simultaneously designing active control of tower vibrations and power control in wind turbines," *Energy Rep.*, vol. 9, pp. 1637–1650, Dec. 2023, doi: 10.1016/j.egyr.2022.12.141.

[34] A. Saenz-Aguirre, E. Zulueta, U. Fernandez-Gamiz, A. Ulazia, and D. Teso-Fz-Betono, "Performance enhancement of the artificial neural network–based reinforcement learning for wind turbine yaw control," *Wind Energy*, vol. 23, no. 3, pp. 676–690, Mar. 2020, doi: 10.1002/we.2451.

[35] Y. Liu, S. Zhang, X. Wang, X. Gao, and T. Cao, "Optimization of torque control parameters for wind turbine based on drive chain active damping control," *IEEE Access*, vol. 10, pp. 106482–106494, 2022, doi: 10.1109/ACCESS.2022.3212155.

[36] Z. Lin, Z. Chen, Q. Wu, S. Yang, and H. Meng, "Coordinated pitch & torque control of large-scale wind turbine based on Pareto efficiency analysis," *Energy*, vol. 147, pp. 812–825, Mar. 2018, doi: 10.1016/j.energy.2018.01.055.

[37] Z. Lin, Z. Chen, J. Liu, and Q. Wu, "Coordinated mechanical loads and power optimization of wind energy conversion systems with variable-weight model predictive control strategy," *Appl. Energy*, vol. 236, pp. 307–317, Feb. 2019, doi: 10.1016/j.apenergy.2018.11.089.

[38] D. Song, Y. Tu, L. Wang, F. Jin, Z. Li, C. Huang, E. Xia, R. M. Rizk-Allah, J. Yang, M. Su, and Y. Hoon Joo, "Coordinated optimization on energy capture and torque fluctuation of wind turbines via variable weight NMPC with fuzzy regulator," *Appl. Energy*, vol. 312, Apr. 2022, Art. no. 118821, doi: 10.1016/j.apenergy.2022.118821.

[39] A. Gambier and A. Behera, "Integrated pitch control system design of a wind turbine by using multiobjective optimization," *IFAC-PapersOnLine*, vol. 51, no. 28, pp. 239–244, 2018, doi: 10.1016/j.ifacol.2018.11.708.

[40] M. Lara, J. Garrido, M. L. Ruz, and F. Vázquez, "Adaptive pitch controller of a large-scale wind turbine using multi-objective optimization," *Appl. Sci.*, vol. 11, no. 6, p. 2844, Mar. 2021, doi: 10.3390/app11062844.

[41] A. Gambier, "Multiobjective optimal control of wind turbines: A survey on methods and recommendations for the implementation," *Energies*, vol. 15, no. 2, p. 567, Jan. 2022, doi: 10.3390/en15020567.

[42] A. Ghasemkhani, S. Farahat, and M. M. Naserian, "Multi-objective optimization and decision making of endoreversible combined cycles with consideration of different heat exchangers by finite time thermodynamics," *Energy Convers. Manage.*, vol. 171, pp. 1052–1062, Sep. 2018, doi: 10.1016/j.enconman.2018.06.046.

[43] J. Sarshar, S. S. Moosapour, and M. Joorabian, "Multi-objective energy management of a micro-grid considering uncertainty in wind power forecasting," *Energy*, vol. 139, pp. 680–693, Nov. 2017, doi: 10.1016/j.energy.2017.07.138.

[44] T. Li, A. Li, and X. Guo, "The sustainable development-oriented development and utilization of renewable energy industry—A comprehensive analysis of MCDM methods," *Energy*, vol. 212, Dec. 2020, Art. no. 118694, doi: 10.1016/j.energy.2020.118694.

[45] E. Lozano-Minguez, A. J. Kolios, and F. P. Brennan, "Multi-criteria assessment of offshore wind turbine support structures," *Renew. Energy*, vol. 36, no. 11, pp. 2831–2837, Nov. 2011, doi: 10.1016/j.renene.2011.04.020.
[46] P. Wang, Z. Zhu, and Y. Wang, "A novel hybrid MCDM model combining the SAW, TOPSIS and GRA methods based on experimental design," *Inf. Sci.*, vol. 345, pp. 27–45, Jun. 2016, doi: 10.1016/j.ins.2016.01.076.
[47] E. Gaertner, *Definition of the IEA Wind 15-Megawatt Offshore Reference Wind Turbine Technical Report*, document NREL/TP-5000-75698, 2020, Accessed: Apr. 24, 2023. [Online]. Available: www.nrel.gov/publications
[48] NREL. (2023). *OpenFAST v3.4.1 Documentation*. Accessed: Apr. 24, 2023. [Online]. Available: https://openfast.readthedocs.io/en/main/
[49] R. Niranjan and S. B. Ramisetti, "Insights from detailed numerical investigation of 15 MW offshore semi-submersible wind turbine using aero-hydro-servo-elastic code," *Ocean Eng.*, vol. 251, May 2022, Art. no. 111024, doi: 10.1016/j.oceaneng.2022.111024.
[50] F. Papi and A. Bianchini, "Technical challenges in floating offshore wind turbine upscaling: A critical analysis based on the NREL 5 MW and IEA 15 MW reference turbines," *Renew. Sustain. Energy Rev.*, vol. 162, Jul. 2022, Art. no. 112489, doi: 10.1016/j.rser.2022.112489.
[51] J. Jonkman, S. Butterfield, W. Musial, and G. Scott. (2009). *Definition of a 5-MW Reference Wind Turbine for Offshore System Development*. Accessed: Apr. 24, 2023. [Online]. Available: http://www.osti.gov/bridge
[52] L. Pustina, J. Serafini, C. Pasquali, L. Solero, A. Lidozzi, and M. Gennaretti, "A novel resonant controller for sea-induced rotor blade vibratory loads reduction on floating offshore wind turbines," *Renew. Sustain. Energy Rev.*, vol. 173, Mar. 2023, Art. no. 113073, doi: 10.1016/j.rser.2022.113073.
[53] C.-J. Chueh, C.-H. Chien, C. Lin, T.-Y. Lin, and M.-H. Chiang, "Dynamic co-simulation analysis and control of an IEA 15 MW offshore floating semi-submersible wind turbine under Taiwan offshore-wind-farm conditions of wind and wave," *J. Mar. Sci. Eng.*, vol. 11, no. 1, p. 173, Jan. 2023, doi: 10.3390/jmse11010173.
[54] J. Jonkman, "The new modularization framework for the FAST wind turbine CAE tool," in *Proc. 51st AIAA Aerosp. Sci. Meeting Including New Horizons Forum Aerosp. Expo.*, Jan. 2013, p. 202, doi: 10.2514/6.2013-202.
[55] J. M. Jonkman, *Dynamics Modeling and Loads Analysis of an Offshore Floating Wind Turbine*. Golden, CO, USA: National Renewable Energy Lab. (NREL), Dec. 2007, doi: 10.2172/921803.
[56] B. J. Jonkman. *Turbsim User's Guide: Version 1.50*. Golden, CO, USA, Sep. 2009, doi: 10.2172/965520.
[57] IEC 61400-1. (2005). *Wind Turbines—Part 1: Design Requirements*. Accessed: Apr. 24, 2023. [Online]. Available: www.iec.ch/searchpub
[58] N. J. Abbas, D. S. Zalkind, L. Pao, and A. Wright, "A reference open-source controller for fixed and floating offshore wind turbines," *Wind Energy Sci.*, vol. 7, no. 1, pp. 53–73, Jan. 2022, doi: 10.5194/wes-7-53-2022.
[59] (Oct. 2012). *NREL, MLife*. Accessed: Apr. 24, 2023. [Online]. Available: https://www.nrel.gov/wind/nwtc/mlife.html

**MANUEL LARA** was born in Ciudad Real, Spain, in 1991. He received the B.S. and M.S. degrees in industrial electronics engineering and industrial engineering from the University of Cordoba, Cordoba, Spain, in 2015 and 2017, respectively, and the M.S. degree in systems and control engineering from National Distance Education University, Madrid, Spain, in 2018.

Since 2018, he has been a Predoctoral Fellow FPU funded by the Ministry of Science, Innovation and Universities Spain, Department of Electrical Engineering and Automation, University of Cordoba. He is currently participating in several research and development projects obtained in regional and national competitive public grants. His research interest includes wind turbine control.

**FRANCISCO VÁZQUEZ** was born in Cordoba, Spain, in 1968. He received the M.S. and Ph.D. degrees in physics from National Distance Education University, Madrid, Spain, in 1995 and 2001, respectively.

From 1999 to 2002, he was an Assistant Professor with the Computer Science Department, University of Cordoba. Since 2003, he has been an Associate Professor with the University of Cordoba, where he is currently with the Department of Electrical Engineering and Automation. His research interests include control systems, multivariable control, wind turbines, HVAC systems, and the advanced methodologies of simulation and modeling.

**IÑAKI SANDUA-FERNÁNDEZ** was born in Pamplona, Spain, in 1992. He received the B.S. degree in electric and electronics engineering and the M.S. degree in renewable energies from the Public University of Navarre, Pamplona, in 2014 and 2016, respectively.

Since 2018, he has been a Researcher with the Wind Energy Department, National Renewable Energy Centre of Spain (CENER), specially focused on control systems and load analysis. His research interests mainly include offshore wind turbine control, stability analysis, and the simulation and testing of load cases.

**JUAN GARRIDO** was born in Cordoba, Spain, in 1982. He received the B.S. and M.S. degrees in electronics engineering from the University of Cordoba, Cordoba, in 2004 and 2006, respectively, and the Ph.D. degree in automatic control from National Distance Education University, Madrid, Spain, in 2012.

From 2012 to 2019, he was an Assistant Professor with the Computer Science Department, University of Cordoba, where he has been an Associate Professor with the Department of Electrical Engineering and Automation, since 2019. His research interests include control systems, multivariable control, PID controllers, and wind turbine control.